Nanoelectronics and Its New Materials – A NEW ERA OF NANOSCIENCE

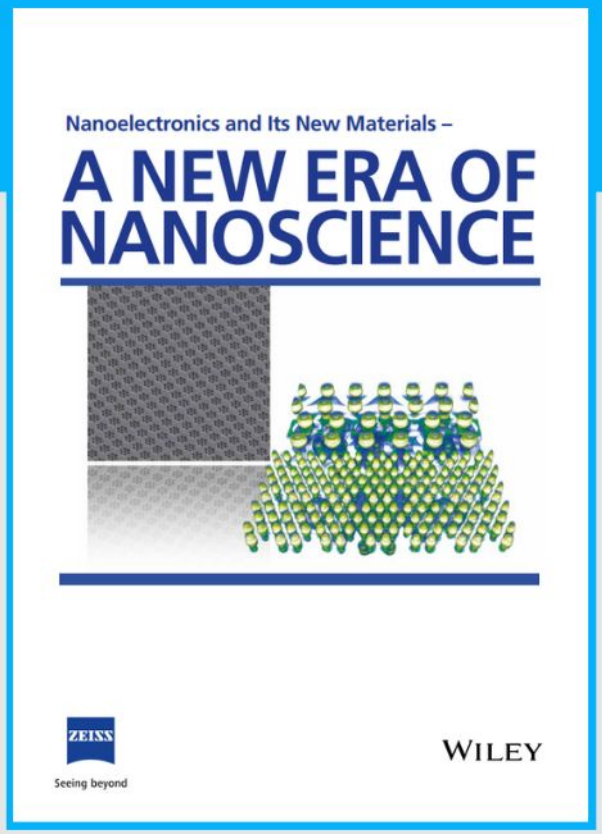

Discover the recent advances in electronics research and fundamental nanoscience.

Nanotechnology has become the driving force behind breakthroughs in engineering, materials science, physics, chemistry, and biological sciences. In this compendium, we delve into a wide range of novel applications that highlight recent advances in electronics research and fundamental nanoscience. From surface analysis and defect detection to tailored optical functionality and transparent nanowire electrodes, this eBook covers key topics that will revolutionize the future of electronics.

To get your hands on this valuable resource and unleash the power of nanotechnology, simply download the eBook now. Stay ahead of the curve and embrace the future of electronics with nanoscience as your guide.

ZEISS

Seeing beyond

WILEY

ADVANCED FUNCTIONAL MATERIALS
www.afm-journal.de

Covalent Protein Immobilization on 3D-Printed Microfiber Meshes for Guided Cartilage Regeneration

Madison J. Ainsworth, Oliver Lotz, Aaron Gilmour, Anyu Zhang, Michael J. Chen, David R. McKenzie, Marcela M.M. Bilek, Jos Malda, Behnam Akhavan, and Miguel Castilho**

Current biomaterial-based strategies explored to treat articular cartilage defects have failed to provide adequate physico-chemical cues in order to guide functional tissue regeneration. Here, it is hypothesized that atmospheric-pressure plasma (APPJ) treatment and melt electrowriting (MEW) will produce microfiber support structures with covalently-immobilized transforming growth factor beta-1 (TGFβ1) that can stimulate the generation of functional cartilage tissue. The effect of APPJ operational speeds to activate MEW polycaprolactone meshes for immobilization of TGFβ1 is first investigated and chondrogenic differentiation and neo-cartilage production are assessed in vitro. All APPJ speeds test enhanced hydrophilicity of the meshes, with the slow treatment speed having significantly less C—C/C—H and more COOH than the untreated meshes. APPJ treatment increases TGFβ1 loading efficiency. Additionally, in vitro experiments highlight that APPJ-based TGFβ1 attachment to the scaffolds is more advantageous than direct supplementation within the medium. After 28 days of culture, the group with immobilized TGFβ1 has significantly increased compressive modulus (more than threefold) and higher glycosaminoglycan production (more than fivefold) than when TGFβ1 is supplied through the medium. These results demonstrate that APPJ activation allows reagent-free, covalent immobilization of TGFβ1 on microfiber meshes and, importantly, that the biofunctionalized meshes can stimulate neo-cartilage matrix formation. This opens new perspectives for guided tissue regeneration.

1. Introduction

Articular cartilage is a hyaline tissue covering the end of articulating joints performing primarily a mechano-protective function; however, this tissue has limited regenerative capacity. Being a high and regular load bearing tissue, it suffers from age and lifestyle dependent degeneration.[1,2] Current clinical options for treating articular cartilage defects include marrow stimulation through microfracture of the subchondral bone and cell-based strategies, in particular autologous chondrocyte implantation (ACI)[3,4] and matrix-assisted autologous chondrocyte implantation (MACI).[5] Cell-based regenerative strategies have been shown to outperform the gold standard microfracture treatment, but they often still result in the formation of a temporary (fibro)cartilaginous tissue that does not possess the same characteristics as the original native cartilage and lacks durable stability.[6] As the new tissue is low in cartilage specific components, like collagen type II and

M. J. Ainsworth, J. Malda, M. Castilho
Regenerative Medicine Centre Utrecht
University Medical Center Utrecht
3584 Utrecht, The Netherlands
E-mail: m.dias.castilho@tue.nl

M. J. Ainsworth, J. Malda, M. Castilho
Department of Orthopedics
University Medical Center Utrecht
3584 Utrecht, The Netherlands

The ORCID identification number(s) for the author(s) of this article can be found under https://doi.org/10.1002/adfm.202206583.

DOI: 10.1002/adfm.202206583

O. Lotz, A. Gilmour, A. Zhang, M. M.M. Bilek, B. Akhavan
School of Biomedical Engineering
University of Sydney
Sydney 2006, Australia
E-mail: behnam.akhavan@sydney.edu.au

O. Lotz, M. M.M. Bilek
School of Aerospace, Mechanical & Mechatronic Engineering
The University of Sydney
Sydney 2006, Australia

O. Lotz, A. Gilmour, D. R. McKenzie, M. M.M. Bilek, B. Akhavan
School of Physics
University of Sydney
Sydney 2006, Australia

A. Gilmour, M. M.M. Bilek
Charles Perkins Centre
University of Sydney
Sydney 2006, Australia

proteoglycans that lack the density and zonal organization of native cartilage, it is much weaker and only provides limited mechanical resilience. This inevitably leads to mechanical failure and problems for the patient in the longer term. Therefore, load-carrying ability together with adequate recruitment and control of differentiation to cartilage-specific cells need to be critically addressed to provide a long-lasting, regenerative solution for the treatment of articular cartilage damage.

Biodegradable support structures have been explored to enhance the stability of cartilage implants, but due to the mechanically challenging environment of the native tissue, relatively large amounts of biomaterial are used, leaving limited space for infiltrating cells and the induction of a regenerative response. Alternative implants based on cell-laden hydrogels reinforced with 3D-printed fibers obtained by melt electrowriting (MEW), have recently shown great potential for the fabrication of mechanically resilient constructs using a lower volume of support biomaterial.[7–9] Interestingly, the use of only small percentages (7%) of highly organized, micrometric sized fibers (made of poly-ε-caprolactone (PCL)) resulted in mechanical characteristics that approximated those of native cartilage.[7] Although these constructs can provide enhanced support, their limited capacity to promote tissue growth and uniform matrix deposition has limited their long-term biomechanical stability.

It is known that cytokines, like transforming growth factor beta (TGFβs), influence chondrogenic differentiation from the early to the final stages of development, play a role in quiescent chondrocyte maintenance, and prevent hypertrophy.[10–12] Therefore, strategies that allow the immobilization of TGFβ to the surface of MEW PCL polymers can open new perspectives to support and guide seeded chondrocytes' differentiation and subsequent cartilage tissue formation. Over the last few decades, extensive research has been performed on wet chemistry approaches for covalent biomolecule attachment to biomaterials. Despite promising results, they share a number of shortcomings that make them unsuitable for regenerative medicine, and in particular cartilage regeneration, such as long reaction times, variable yields, side-reactions, and reagent toxicity.[13–15] Similarly, biomolecules that are weakly bound to polymer surfaces through physical adsorption can be detached too quickly, due to erosion by fluid flow, or displacement through protein exchange.[15–17] Previously, latent TGF complexes were attached to electrospun fibers using low pressure ammonia plasma to elicit a chondrogenic response.[18] The approach was limited by the lack of control over biomolecule placement and damage to the fibers was not thoroughly investigated. Plasma is a complex fluid with multiple species, often described as a conductive gas thanks to its free electrons.[19] When the ions and electrons are out of thermal equilibrium, the plasma is described as 'cold', and typically forms a 'glow discharge'. Recently, a new strategy for the covalent attachment of biomolecules, based on atmospheric pressure plasma (APP), has been introduced.[20] APP devices typically use non-thermal-equilibrium plasma to conduct a variety of surface modifications, such as etching and sterilization within a matter of seconds.[21–23] This is of benefit to softer substrates that are not resistant to thermal stress. When gas flowing through capillaries is ionized by electric fields these devices are referred to as APP jets (APPJs).[21–23] Results have shown that dielectric barrier discharge APP systems[20] and APPJs[24] can be used to activate 2D polymeric surfaces to facilitate on-contact covalent immobilization of extracellular matrix proteins in a single-step, reagent-free process. Furthermore, the potential of APPJs to functionalize 3D polymeric meshes and subsequently covalently immobilize biomolecules without the need for wet chemistry processes has yet to be demonstrated.

Here, we hypothesize that APPJs can be used as a biofunctionalization tool to enable covalent immobilization of TGFβ1 (TGF) biomolecule on 3D microfiber meshes for improved cell interaction and guided cartilage regeneration (**Figure 1**). To test this hypothesis, 3D microfiber meshes of medical grade PCL were generated by melt electrowriting and subsequently activated by APPJ treatment for TGF covalent immobilization. The effects of APPJ treatment on microfiber meshes were systematically studied for surface activation, load-carrying ability properties, and protein immobilization. Further, to determine the potential of immobilized TGF to guide chondrogenic differentiation, an in silico chondrogenesis model was used to complement the subsequent in vitro experiments. These biofunctionalized MEW meshes were seeded with mesenchymal stromal cells (MSCs) and cultured in vitro over 28 days in both basal and chondrogenic medium conditions to assess the activity of the immobilized TGF.

2. Results

2.1. Surface Chemistry and Morphology of APPJ-Treated MEW Microfiber Meshes

Three APPJ treatment speeds were investigated to determine the speed at which the optimal balance between characteristic surface modification and structural deformation is acquired.

M. J. Chen
School of Mathematical Sciences
The University of Adelaide
Adelaide 5005, Australia
M. M.M. Bilek, B. Akhavan
Sydney Nano Institute
University of Sydney
Sydney 2006, Australia
J. Malda
Department of Clinical Sciences
Faculty of Veterinary Medicine
Utrecht University
3584 Utrecht, The Netherlands
B. Akhavan
School of Engineering
University of Newcastle
Callaghan, New South Wales 2308, Australia
B. Akhavan
Hunter Medical Research Institute (HMRI)
New Lambton Heights, New South Wales 2305, Australia
M. Castilho
Department of Biomedical Engineering
Technical University of Eindhoven
5612 Eindhoven, The Netherlands
M. Castilho
Institute for Complex Molecular Systems
Eindhoven University of Technology
5600 MB Eindhoven, The Netherlands

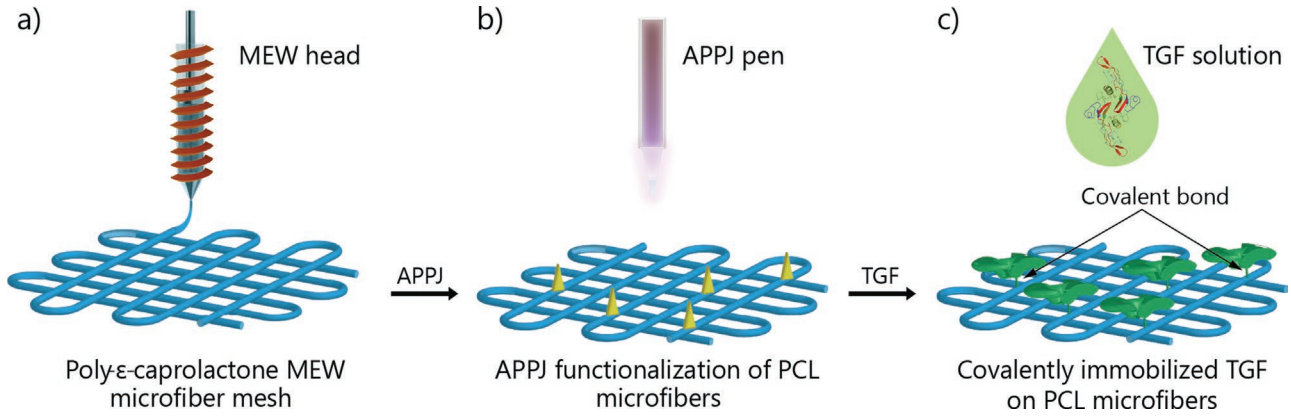

Figure 1. Schematic illustration showing the rationale of the study and covalent immobilization of TGF on PCL MEW microfibers. a) Depiction of PCL MEW microfiber mesh without alteration. b) Representation of MEW mesh following activation with APPJ to add reactive sites, c) Functionalized MEW mesh with TGF covalently immobilized to microfiber surfaces.

These speeds were labeled slow (2.50 m min^{-1}), medium (3.05 m min^{-1}), and fast (3.60 m min^{-1}). The atomic concentrations of carbon and oxygen on meshes did not change with APPJ treatment speeds (i.e., slow, medium, and fast) at the resolution of the XPS survey spectra (**Figure 2**a,c). For example, the average carbon atomic concentrations for the untreated and slow APPJ-treated samples were 75.8 ± 0.3% and 76.6 ± 0.5%, respectively, and those of oxygen were 24.0 ± 0.2% and 23.4 ± 0.5%. Note that hydrogen is not detectable by XPS, because it has no core electrons. No significant amount of nitrogen was detected on either untreated or APPJ-treated meshes. The C1s high-resolution spectra were fitted with compound peaks at binding energies of 284.6 ± 0.5, 286.5 ± 0.5, 287.6 ± 0.5, and 289.0 ± 0.5 eV, corresponding to C−C/C−H, C−O, C=O, and COOH groups, respectively (Figure 2b). The concentration of COOH increased with all APPJ-treatment speeds in comparison to the untreated meshes (Figure 2d). The slow APPJ treatment speed had significantly less C−C/C−H and more COOH than the untreated sample ($p < 0.05$), while the difference was not statistically significant for the fast or medium APPJ treatment speeds. These changes in surface chemistry are attributed to the different time durations for which the MEW microfibers were exposed to plasma. Slower treatment corresponded to longer exposure times, and therefore more time for interactions between the surfaces and reactive species in the plasma. Moreover, the increase of oxygen-containing groups with the increase in treatment time indicates surface oxidation as a result of APPJ treatment. The degree of oxidation may have been small enough as to not be detected by the lower resolution survey scans (Figure 2a), but still be detectable by the higher resolution C1s scans (Figure 2b) as a result of the signal to noise ratio increase.[25] Variations observed in the COOH concentration for treated samples are within the experimental error of XPS measurements, in particular for small spot size measurements performed on thin fibers. This variability does not affect the conclusions made from the XPS results.

To further understand the effect of the APPJ treatment speeds on the surface oxidation and hydrophilicity of MEW meshes, the dynamic wettability was characterized (Figure 2e). All treated conditions displayed increased hydrophilicity compared to the untreated, as demonstrated by water drops being drawn into the meshes. The drops placed on fast APPJ-treated meshes tended to remain outside the mesh (≈15 s) before being drawn in gradually (30—60 s). Therefore, after 60 s from when the drop was originally placed there tended to be a small amount left, that disappeared by 180 s. However, those on the slow APPJ-treated samples tended to be drawn in earlier (<5 s) and quicker (<30 s), but not always drawn in completely. This meant that despite the speed with which the drops were drawn in, there was often a proportion of the original drop left on the mesh's surface after 180 s. The drops placed on medium APPJ-treated samples tended to be drawn in either quickly or gradually. However, the medium APPJ-treated samples were unlike the slow in that the whole drop tended to be drawn into the mesh. The images selected for the medium APPJ-treated condition display a drop drawn in quickly (<30 s). These qualitative results indicate that, independent of the APPJ treatment speed, hydrophilicity of the MEW meshes was substantially increased.

In addition, the effect of APPJ treatment speeds on MEW meshes' morphology and mechanical performance was studied. Morphological changes from the untreated condition were observed only on the slow-APPJ-treated sample (**Figure 3**a; Figure S2, Supporting Information). The surface of the fibers had increased roughness and some fibers displayed fusing. Moreover, these changes appeared to decrease in severity toward the core of the meshes, moving down in the out-of-plane printing direction (i.e., direction of laid-down fibers). Importantly, no significant differences were observed between the tensile moduli of the MEW meshes APPJ-treated at different speeds, nor between those and the MEW meshes that were not exposed to APPJ (Figure 3b). This indicates that the morphological changes induced by APPJ seem to not result in a significant alteration of the mechanical performance of the meshes under uniaxial tensile loading.

2.2. TGF Immobilization and Quantification

Confirmation and quantification of TGF immobilization was subsequently investigated using immunofluorescent imaging and ELISA. TGF retention on microfibers was additionally investigated using ELISA. Immunofluorescent detection of

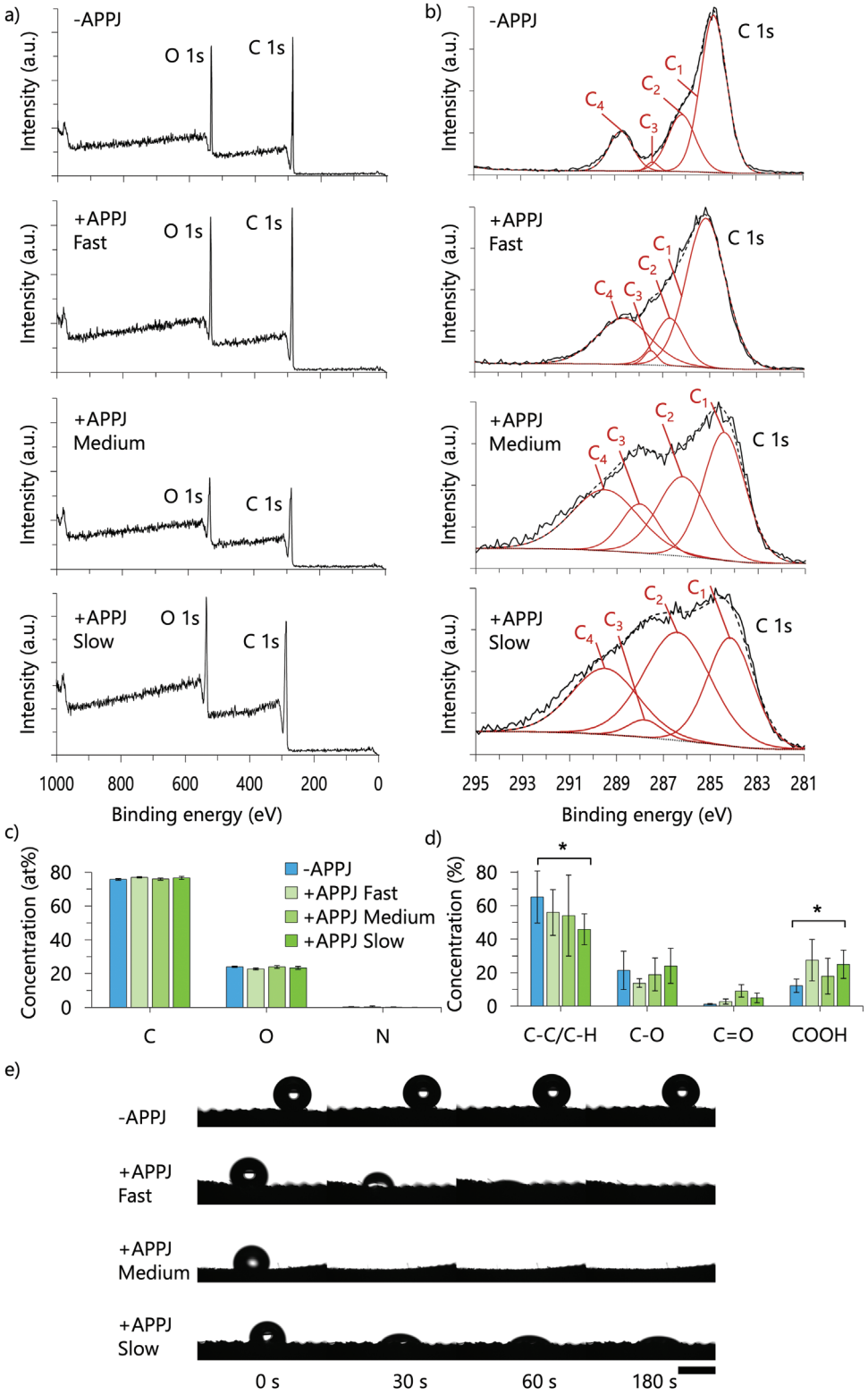

Figure 2. Effect of APPJ treatment on surface chemistry of PCL MEW microfiber meshes. a) XPS survey spectra taken after treatment with various APPJ treatment speeds. c) Curve fitted XPS C1s high resolution spectra obtained for samples prepared using various APPJ treatment speeds. The spectra are curve fitted by four components: C1, C—C/C—H; C2, C—O; C3, C=O; C4, COOH. The dashed curve indicates fit. c) Carbon I, oxygen (O), and nitrogen (N) atomic concentrations for samples treated with various APPJ speeds. d) Atomic concentration of peak-fitted C 1s components for various APPJ treatment speeds. APPJ treatment increased the prevalence of C—O, C=O, and COOH groups. XPS data; $n = 2$ (5x technical replicates). Data (c,d) presented as mean ± SD. Paired T test for significance with p-values ≤ 0.05 = *. e) Selected images of the dynamic wettability of meshes after various APPJ treatment speeds at various times after drop placement. Water drops were not drawn into the untreated meshes, but were drawn into the treated meshes. $n \geq 2$ (3x technical replicates). Representative images shown. Scale bar (bottom right) = 2 mm.

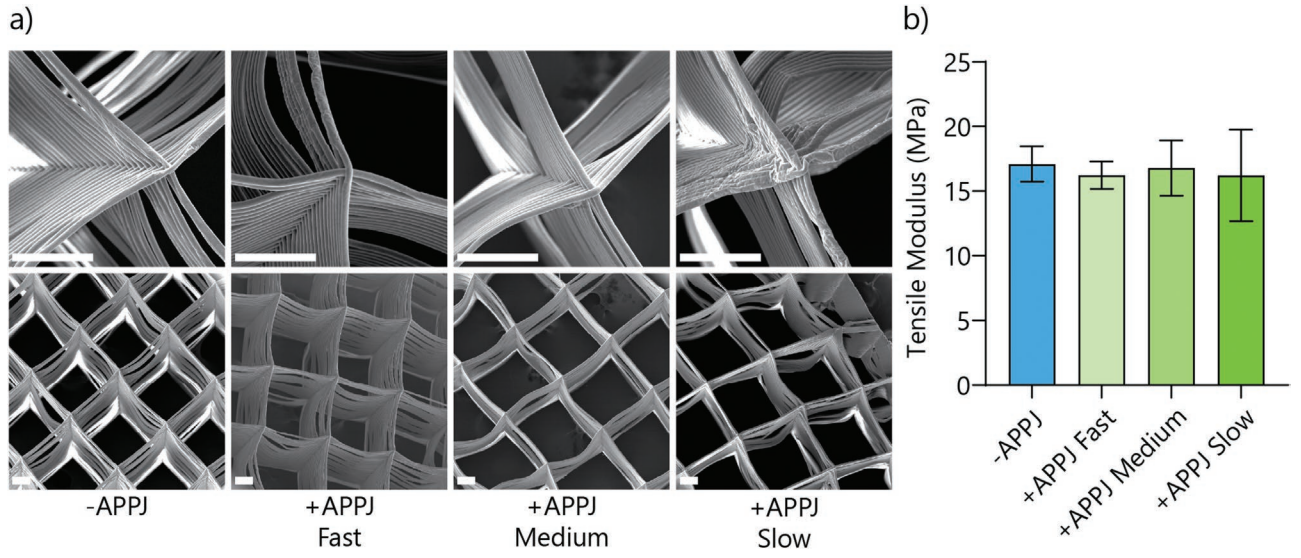

Figure 3. Effect of APPJ treatment on PCL MEW microfiber mesh morphology. a) SEM images of meshes after various APPJ treatment speeds (SE detector). $n = 1$. Scale bars = 100 µm. b) Uniaxial tensile test results of MEW meshes without APPJ treatment and after fast-, medium-, and slow-speed APPJ treatment. Data displayed as mean ± SD. $n = 3$. One-way ANOVA with Tukey's multiple comparisons revealed no statistical difference ($p > 0.05$).

TGF confirmed the presence of biomolecule attachment to MEW microfiber meshes (**Figure 4**a). Higher signal intensities are correlated with higher protein immobilization concentrations. Markedly, there was a significant increase in the total pixel value of the APPJ treated meshes when compared to the untreated ones. This increase was ≈44-fold for the 10 ng mL^{-1} and almost twofold for the 1000 ng mL^{-1} group. Protein within the MEW mesh could also be detected for the untreated group immersed in 1000 ng mL^{-1}. This can be potentially related to the physical adsorption of TGF protein to the hydrophobic MEW fibers. It is expected that this physically absorbed protein would be removed with a more rigorous washing protocol.

An ELISA assay was used to quantitatively investigate the presence of various TGF concentrations on PCL MEW microfiber meshes (Figure 4b). The higher the TGF concentration, the higher the signal for all APPJ-treated conditions. Further, the ELISA signal for APPJ-treated conditions with 2000, 1000, and 500 ng mL^{-1} TGF were all significantly greater than that for the untreated condition even when the untreated sample was incubated with the highest concentration of the protein solution, 2000 ng mL^{-1} ($p \leq 0.0001$). The untreated conditions did not display a signal significantly different from background (p~1). This equivalence to background indicates that the TGF signals observed in treated conditions corresponded to covalently bound TGF. Moreover, no significant difference was observed in ELISA signals obtained for the meshes APPJ-treated at various speeds and incubated with the same TGF concentration. This lack of variation with exposure time indicates that the exposure time to APPJ had no significant influence on the efficacy of covalent immobilization. Although the slower speed resulted in higher treatment intensity, as indicated by surface chemistry, morphology, and wettability results (Figures 2 and 3), the effect of APPJ speed may not have been large enough to be detected by the ELISA experiment. Alternatively, the density of reactive sites imparted in the weakest treatment may have been high enough that the amount of protein bound was limited by its diffusion to the surface from the solution rather than by availability of reactive sites. Based on the improved hydrophilic behavior, only the slow-APPJ-treated meshes were continued for further evaluation.

Further ELISAs were conducted to determine the immobilization efficiency and elution of TGF on treated and untreated scaffolds. Significantly lower amounts of TGF were found to remain in the solutions after incubation with APPJ-treated meshes compared to those incubated with untreated meshes (Figure 4c). The loading efficiency for untreated meshes was calculated to be 52.4 ± 3.6%, while that of the APPJ-treated meshes was 82.1 ± 0.1%. The average density of TGF was calculated to be 0.75 ± 0.05 ng mm^{-2} on untreated and 1.182 ± 0.001 ng mm^{-2} on APPJ-treated meshes. ELISA measurements of TGF on scaffolds underscore the observation that APPJ-treated meshes loaded significantly more TGF after incubation than the untreated ones (Figure 4d). In addition, less TGF was released from APPJ-treated meshes than untreated meshes over a 28 day period with multiple changes of media (Figure 4c). Approximately 55.4 ± 3.1% of the TGF loaded onto untreated meshes was retained after the 28 days, whereas, 81.9 ± 1.9% was retained on the APPJ-treated meshes. The results demonstrate that the APPJ-treated scaffolds increase TGF loading efficiency and retention, and therefore, APPJ-treated meshes provide the corresponding biochemical cues at higher rates and for longer periods of time.

2.3. In Vitro Chondrogenic Differentiation and Neo-Cartilage Formation in Surface Activated MEW Meshes

Activity of immobilized TGF was investigated using in vitro experimentation. The –APPJ +TGF condition under the following evaluation was considered the gold standard approach for chondrogenic differentiation of MSCs in vitro that entails supply of freshly thawed TGF to the cells at each media change.

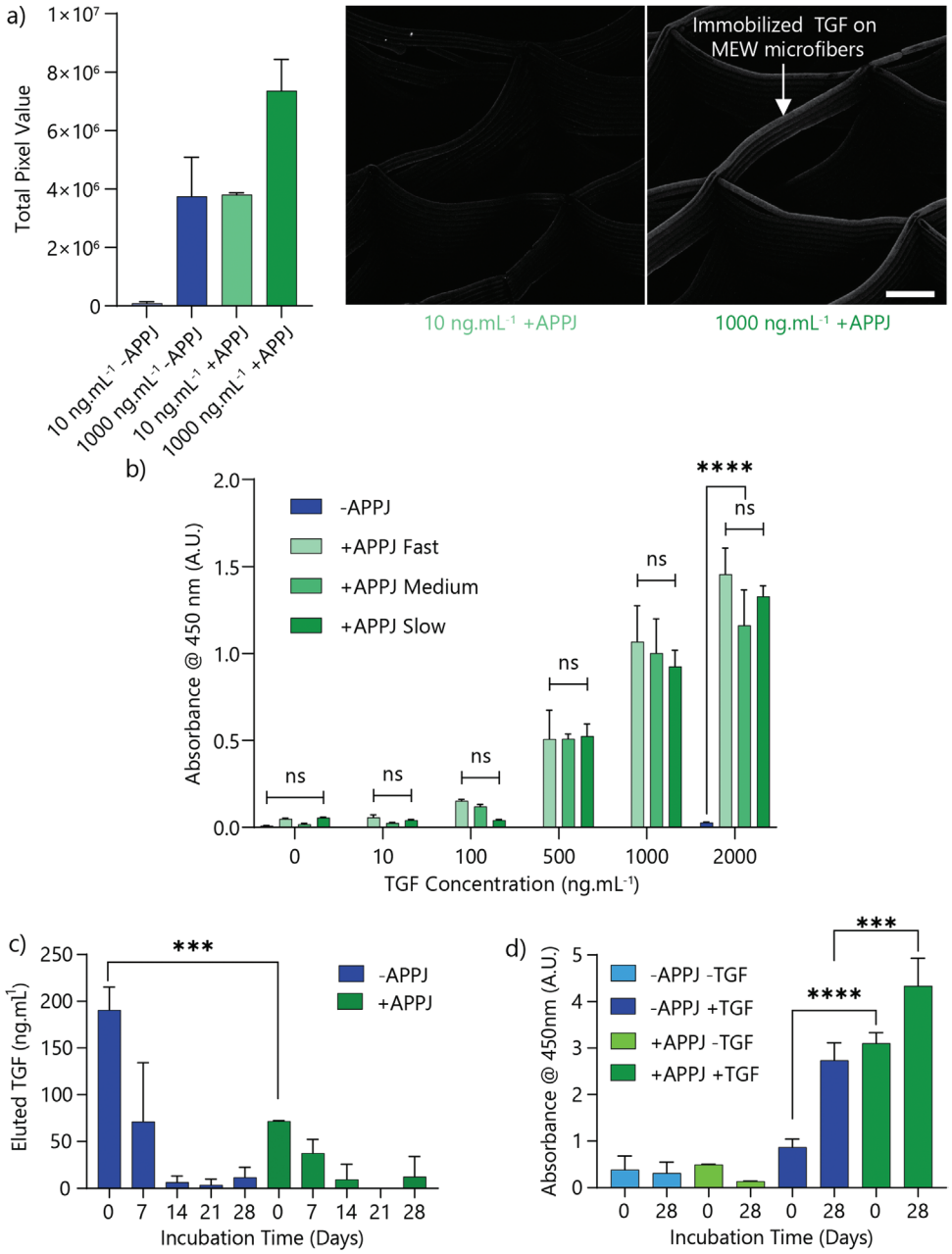

Figure 4. TGF immobilization and quantification. a) Counted total pixel values to represent fluorescence intensity with accompanying immunofluorescent staining of immobilized TGF (10 and 1000 ng mL^{-1}) on APPJ-functionalized MEW microfiber meshes after mild detergent washing. Scale bar = 100 µm. $n = 2$. Data presented as mean ± SD. b) Quantification of protein attachment to MEW microfiber meshes using ELISA after rigorous detergent washing. $n = 3$. Data presented as mean ± SD. c) Concentration of TGF eluted from untreated and APPJ-treated meshes after TGF immobilization by incubation in 1000 ng mL^{-1} TGF containing solution. The measurement for day zero (0) is the residual TGF remaining in the incubation solution after immobilization. $n = 3$. Data presented as mean ± SD. d) ELISA (absorbance at 450 nm) of immobilized TGF retained on meshes with and without TGF immediately after incubation (0) and after 28 days. The buffer solution was changed every 7 days. $n = 3$. Data presented as mean ± SD. Bonferroni's post hoc test for significance. (ns) $p > 0.5$, (*) $p \leq 0.05$, (**) $p \leq 0.01$, (***) $p \leq 0.001$, (****) $p \leq 0.0001$.

Preliminary in vitro optimization of protein immobilization and subsequent MSC differentiation and neo-cartilage tissue formation was performed with varying concentration of protein immersion solutions of TGF (**Figure 5**). In vitro results revealed that lower concentrations of immobilized TGF (<1000 ng ml^{-1}) did not promote sufficiently observed cellular infiltration and homogenous neo-cartilage matrix production (Figure 5c), despite the lack of significance in normalized GAG production between treatment groups (Figure S3, Supporting Information). Hence, the slow APPJ treatment speed in combination with the 1000 ng mL^{-1} concentration for immobilization was used for the forthcoming in vitro analysis.

It was found that the groups with TGF (whether immobilized on the surface or dissolved in the medium), had consist-

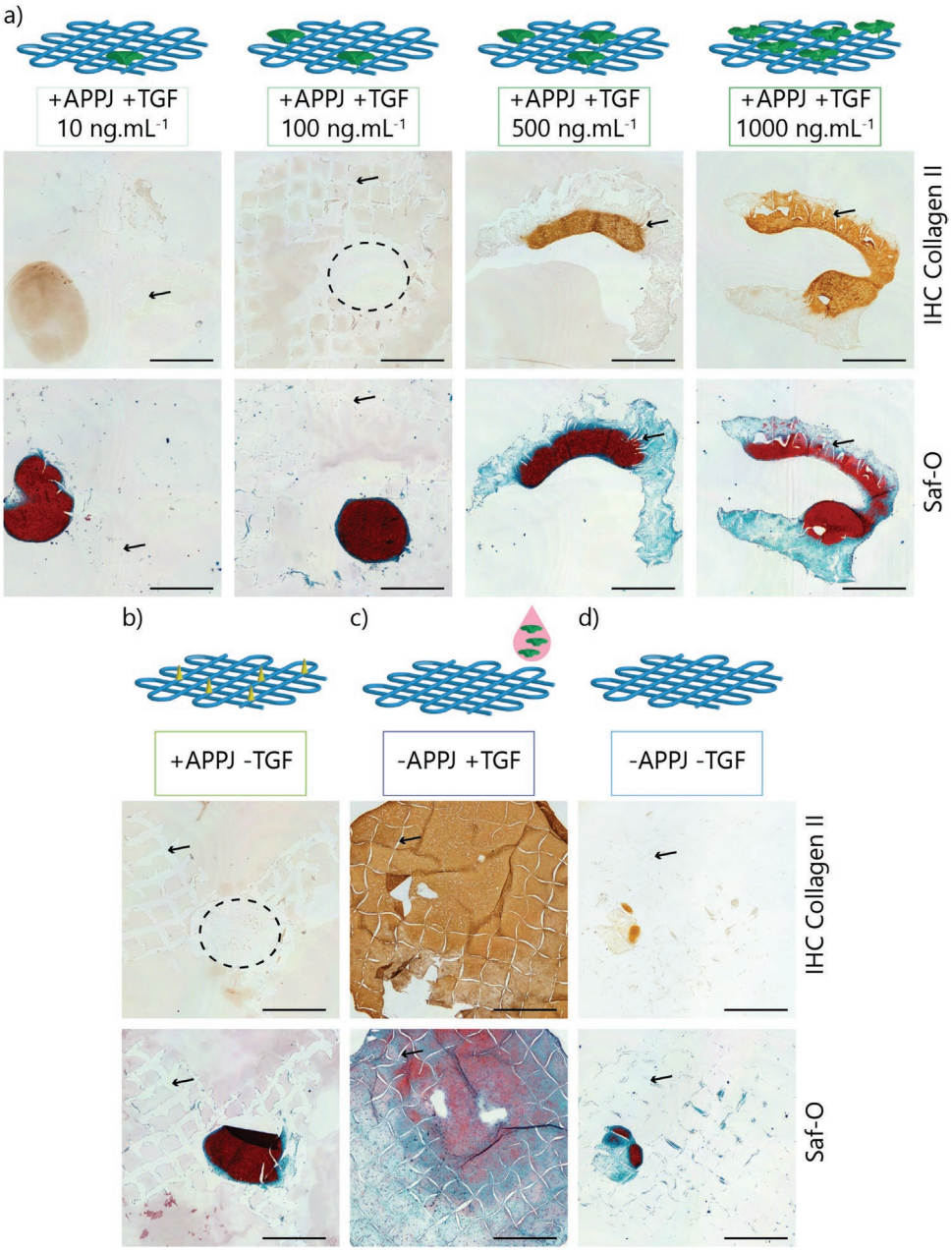

Figure 5. Effect of TGF protein supplementation strategy and concentration on chondrogenic differentiation of seeded MSCs and neo-cartilage formation. Schematic with representative in vitro histological analysis of cartilage-like matrix deposition. a) Treatment groups with varied concentrations of immobilized TGF to the APPJ-functionalized surfaces. b) Group activated with APPJ treatment, but without TGF supplementation. c) Group without functionalization, but with TGF supplied 2x per week in the culture medium at 10 ng mL^{-1}. d) Group without APPJ functionalization nor TGF supplementation. Blue lines indicate MEW fibers, green shapes indicate TGF, and yellow shapes indicate reactive sites. Dashed circles indicate location of displaced pellet-like structures. Arrows indicate MEW microfibers dissolved during histological processing. Scale bars = 1 mm. $n = 2$.

ently higher metabolic activity in comparison to the groups without TGF supplied (**Figure 6**a), noting that the readings were not normalized against DNA content in order to make the measurements on the same samples throughout the culture period. In addition, glycosaminoglycan (GAG) production was observed to significantly increase following 28 days in culture in the +APPJ +TGF group and was considerably elevated at the end of the culture period compared to the other groups (Figure 6b). Clear trends of increasing GAG production were observed throughout the culture period in the –APPJ +TGF group. Treatment groups without immobilization or supplementation in culture medium of TGF displayed GAG production with more variability and less consistency than the other groups over the culture period (Figure 6b).

To confirm neo-cartilage ECM deposition, mechanical properties of cultured meshes were characterized under uniaxial compression loading (Figure 6c). Compression tests carried out on cultured meshes on day 28 of culture revealed similar

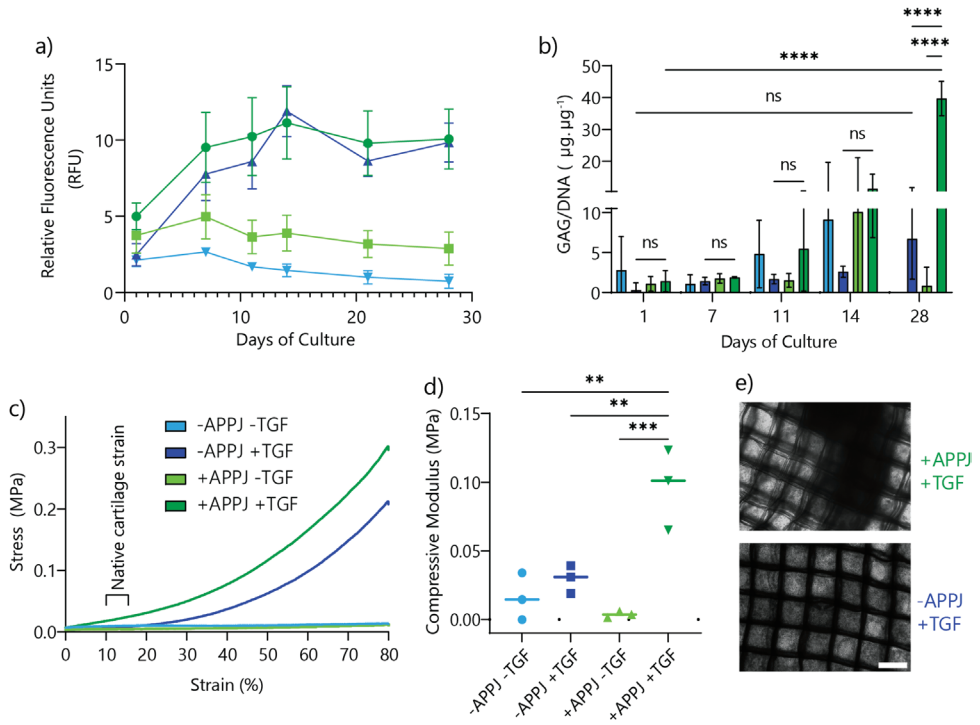

Figure 6. MSCs seeded in biofunctionalized MEW microfiber meshes with TGF undergo chondrogenic differentiation and support neo-cartilage formation. a) Progressive metabolic activity of cultured meshes using resazurin assay, $n = 6$. Data presented as mean ± SD. b) GAG production, normalized against DNA quantity, of meshes throughout the culture period, $n = 6$. Data presented as mean ± SD. Two-way ANOVA with Tukey's multiple comparisons for significance. c) Representative engineering stress–strain curves with d) compressive modulus determined in the physiological native articular cartilage strain region $n = 3$ (individual values plotted with mean). Two-way ANOVA with Tukey's multiple comparisons for significance. e) Accompanying brightfield images of cultured meshes on D28 of in vitro culture (scale bar = 400 µm). (ns) $p > 0.5$, (*) $p \leq 0.05$, (**) $p \leq 0.01$, (***) $p \leq 0.001$, (****) $p \leq 0.0001$.

stress–strain behavior between groups cultured in the presence of TGF (Figure 6c), and statistically ($p < 0.05$) a higher compressive modulus in the +APPJ +TGF group compared to the other three groups (Figure 6d). This finding confirmed the higher density of neo-cartilage ECM components deposited by the seeded MSCs in this group of cultured meshes. Likewise, brightfield imaging carried out progressively on meshes in culture, demonstrated the higher density and more uniform matrix production in the +APPJ +TGF group (Figure 6e).

Furthermore, histological analysis of 3D-cultured meshes was performed to detect deposition of cartilage components (**Figure 7**). The treatment groups without TGF supplementation (+APPJ –TGF, –APPJ –TGF) showed minimal evidence of neo-cartilage matrix production over the culture period (Figure S4, Supporting Information). In contrast, 3D MEW meshes supplemented with TGF (immobilized or in medium) confirmed that these groups were able to support neo-cartilage matrix production. Notably, the treatment group with immobilized TGF (+APPJ +TGF) exhibited production of collagen type II and GAGs following 1 week in culture (D7), whereas these ECM components do not appear in the sections of the TGF supplemented in medium group (–APPJ +TGF) until the second week of culture (Figure 7). Moreover, at D28 of in vitro culture, the +APPJ +TGF group exhibited a higher density of GAGs produced within the sample in comparison to the –APPJ +TGF group. Collagen type I was also detected, but was less prominent.

Quantitative PCR analysis revealed an increased fold change in the +APPJ +TGF and –APPJ +TGF groups in the day 11 and 14 timepoints for COL1A1, COL2A1, SOX9, and ACAN, in comparison to the other treatment groups (**Figure 8**). This finding can be associated with the increase in matrix production (GAGs, collagen I and II) observed most prominently in the +APPJ +TGF group, as well as less pronounced in the –APPJ +TGF group (Figure 7). In addition, the +APPJ +TGF group exhibited a trend of upregulation across the COL2A1, SOX9, and ACAN genes from D1 until D14, and subsequently dropped at D28. COLXA1 was initially upregulated in all groups at D1, however did not exhibit fold change throughout the remainder of the experimental period. The chondrogenic index (COL2A1/COL1A1) was calculated using the treatment group means and revealed that at day 14, the +APPJ +TGF group had a chondrogenic index of 2.32, while the –APPJ +TGF group's chondrogenic index was 0.96.

3. Discussion

With cell-laden approaches for cartilage regeneration, it is imperative that the biomaterials used are able to promote deposition of tissue-specific ECM components and simultaneously ensure sufficient load-carrying ability. MSC differentiation into cartilage cells and subsequent ECM matrix deposition can be facilitated by endogenous growth factors, such as TGF;[10,26]

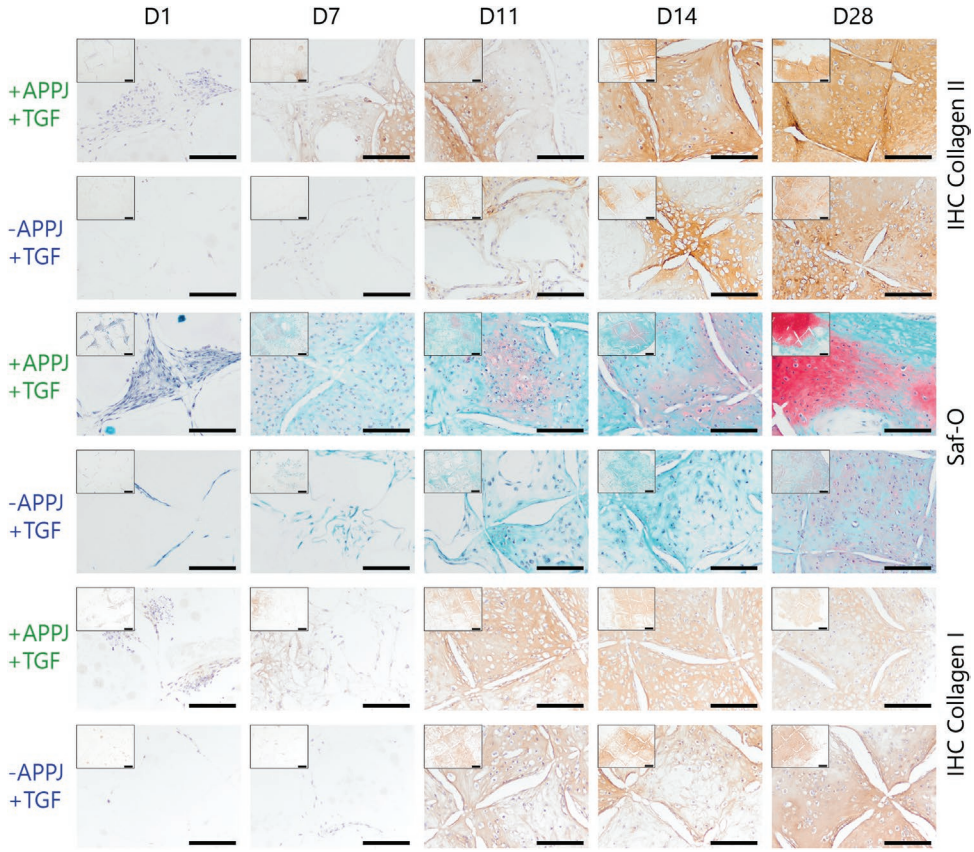

Figure 7. Histological analysis of neo-cartilage components (collagen types I and II, safranin-O) produced in biofunctionalized (+APPJ +TGF) and media-supplemented (–APPJ +TGF) MEW microfiber meshes throughout 28 days of culture. Scale bars = 200 µm. Representative image shown. $n = 2$.

while load-carrying ability of cell-laden biomaterials can be provided by well-organized fiber reinforcing meshes obtained by MEW.[7,9] Here, we discuss our findings for covalently attaching TGF on MEW fiber meshes using APPJ, and demonstration of the potential for this biomaterial system to support and promote neo-cartilage ECM deposition.

For controlling TGF attachment on the surface of MEW fiber meshes, slow APPJ-treatment speed, and correspondingly longer treatment times, was found to be beneficial. Despite a high intra-group variability, this treatment speed resulted in increased dynamic wettability and hydrophilicity when compared to medium and fast speed APPJ-treatments. These findings align with previous works involving APP treatment of substrates composed of PCL[27,28] and other polymers.[13,29] The oxygen containing groups (C—O, C=O, and COOH), have previously been observed to increase on compressed, solvent-casted, and solution electrospun PCL substrates treated with atmospheric pressure[27,28,30] and low pressure plasmas using gas mixtures with[27,28,31] and without[27,28,30] oxygen. However, the proportions of species introduced vary across studies, which is likely due to variations in treatment parameters.

In addition, the variable behavior of drops within the medium APPJ treatment condition may indicate a transition state between the dynamic wettabilities of the fast and slow APPJ treatment conditions. Typically, hydrophilic enhancement is due to the introduction of polar or radical groups from treatment.[21,30,32,33] Further variability in dynamic wettability and contact angles could be a result of factors such as differences in exact drop placement position in relation to the MEW mesh (i.e., pore size and fiber interconnections), from drops being in either the Wenzel or Cassie-Baxter state[34] and from fiber roughness.[35,36] The importance of optimizing between treatment intensity and the lack of deformation has been discussed previously.[37,38] One of the most important factors for the transfer of thermal energy from APPJ plumes is the distance to the substrate.[39] For the purposes of this study, maximizing treatment intensity, with slower treatment speeds, was more important than minimizing morphological changes. In fact, morphological changes on MEW meshes had little or no effect on microfiber mesh load-carrying ability as demonstrated by the uniaxial tensile test.

When the surfaces of MEW PCL fibers were treated at slower APPJ speed, a uniform distribution of protein was observed throughout the mesh. This may be a result of increased fiber hydrophilicity and potential C=O bond breakage[25] that allowed for rapid protein immobilization via covalent attachment of TGF to hydroxyl functional groups at the PCL surface after APPJ treatment. For the medium and fast APPJ treatments, the PCL fiber surface had fewer O-containing groups present and thus less hydrophilic behavior, likely leading to a lower protein immobilization density. In addition, the enhanced hydrophilicity resulted in increased solution and cellular

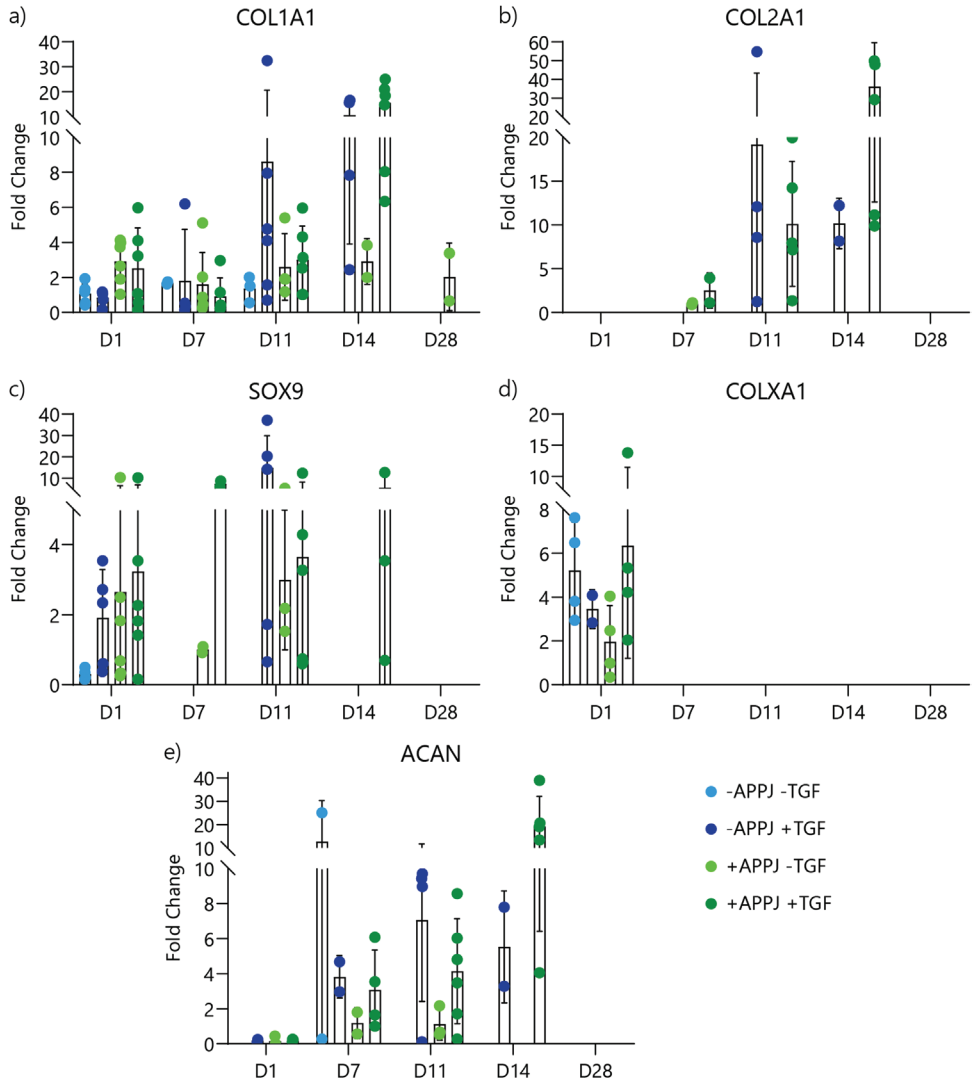

Figure 8. Relative gene fold expression of chondrogenic genes against HPRT (HKG) of MSCs seeded in MEW meshes throughout 28 days of culture. a) Collagen type 1, b) collagen type 2, c) SOX9, d) collagen type 10, and e) aggrecan. Data presented as mean with individual values plotted. Error bars represent standard deviation. $n = 6$.

infiltration into the APPJ-treated meshes measured using real-time-observation, leading to a more efficient protein loading and cell seeding process. As such, an approximately uniform distribution of biochemical signaling and cell response was observed throughout treated scaffolds.

Interestingly, it was observed that the meshes displayed higher protein signals with ELISA when measured 28 days after initial TGF incubation, including buffer changes every 7 days, than when measured on day 0 ($p < 0.01$ for the –APPJ +TGF group). These increased signals for both conditions may be a result of multiple factors affecting the interactions between the TGF and the antibodies used for the ELISA. First, there may be increased physisorption of TGF previously released from the surfaces as a result of PCL swelling and degradation with time in solution. During the development of the protocol for the first ELISA, it was observed that protein adhesion on PCL meshes after 24 h incubation at 4 °C was significantly enhanced than that after 2 h at 24 °C. Typically, these incubation protocols are considered equivalent immobilization alternatives. PCL is known to be a biodegradable polymer,[40,41] experiencing roughening and erosion in water,[42] and possible swelling.[43] Therefore, it is plausible to suggest that the PCL may be degrading with the extra time in solution, presenting new surfaces and cavities that could adsorb and/or trap protein molecules from solution, including the TGF and ELISA antibodies. Second, the hydrophilicity of the meshes would affect the rates of infiltration into the meshes for biomolecules and the solutions, as well as encourage different presentations of the TGF as a result of different electrostatic interactions with the surface. High variability in proteoglycan and GAG production was observed in vitro for untreated meshes, consistent with high variability in their protein loading efficiency. Future experiments should investigate the consistency of protein loading efficiency and bioactivity over time in order to ensure a reliable process for end-use applications.

While the concentration of immobilized TGF is supra-physiological, the APPJ-treated scaffolds with no TGF (+APPJ –TGF)

or concentrations lower than 1000 ng mL^{-1} revealed pellet-like formations of densely packed cells not integrated within the mesh, which exhibited high proteoglycan deposition. This formation can be explained by cellular density (and in turn, MSC stiffness that can influence chondrogenesis) in combination with the chondrogenic factors within the growth medium.[44]

Independently of the protein attachment efficiency, the immobilized TGF on MEW meshes was revealed to be active throughout the 28 days of in vitro cell culture, as demonstrated by its capacity to promote MSC differentiation and deposition of cartilage specific ECM components, like GAGs and Type II collagen. This is a notable achievement for stably coupling endogenous TGF, and potentially other biomolecules, to 3D-printed polymeric structures through a simple, reagent-free process. Previous works in which chemical functional groups, such as NH_2 or COOH, are created on other polymeric materials using depositing processes have demonstrated increases in cell adhesion[45,46] and the promotion of osteogenesis.[29,46] However, no APPJ has previously been used in combination with 3D microfiber meshes, nor to promote chondrogenesis with the immobilization of biomolecules such as TGF, nor to covalently immobilize biomolecules without reagents or wet chemistry processes.

Future works will require further optimization of TGF concentrations or even combination of covalently incorporated biological cues like TGF, or other cytokines, with physical stimulation, e.g., by exposing meshes to mechanical loading during in vitro culture as it is known to boost endogenous TGF production by chondrocytes.[7,47] To further validate the findings of this study, an appropriate in vivo model should be implemented to test the hypothesis, noting the need for optimization of post-surgical mesh integration. Importantly, our findings on the covalent immobilization of TGF biomolecules to high resolution fiber meshes enable us to avoid the limitation of using super physiological amounts of growth factors during in vitro cartilage culture, that would incur high costs and adverse reactions, and finally overcome the limitations of wet chemistry surface treatment strategies and existing plasma technologies.

4. Conclusion

This study demonstrates a novel strategy for the covalent attachment of biomolecules like TGF to 3D-printed polymeric meshes using an APPJ surface treatment. Without diminishing the load-carrying ability of the microfiber mesh and with an increased protein loading efficiency, the APPJ treatment allowed for subsequent, single-step, reagent-free, covalent functionalization of microfiber meshes with TGF. The covalently immobilized TGF retained its bioactivity and induced increased rates of chondrogenic differentiation and neo-cartilage matrix production, compared to a standard protein-in-medium approach. These findings not only have relevance in the field of cartilage regeneration, but also open new perspectives for the design of cell-free, protein-functionalized materials for guided tissue regeneration. The results presented in this paper have important implications, including targeted cellular differentiation and enhanced bioactivity, to the rapidly evolving fields of biofabrication and tissue engineering where the APPJ can be used as a powerful and versatile tool.

5. Experimental Section

Microfiber Mesh Fabrication by Melt Electrowriting: MEW was executed using a 3DDiscovery™ device (RegenHU, Switzerland). Poly-ε-caprolactone (PCL; PURASORB PC12, Corbion, the Netherlands) was melted to 80 °C for 1 h prior to MEW processing. PCL microfiber meshes were fabricated using the following MEW parameters: high voltage 8.14 kV, nozzle size 24G, air pressure 1.26 bar, collector velocity 8 mm s^{-1}, collector distance 6 mm. Square lattice-patterned meshes were fabricated in 50 × 50 mm sheets with fiber spacing of 400 and 500 µm (for in vitro/characterization experiments and immunofluorescent detection, respectively). Meshes used for in vitro experiments were sterilized prior to protein immobilization in 70% ethanol for 30 min and then treated with UV light for 20 min per side.

Atmospheric Pressure Plasma Jet (APPJ) Functionalization of MEW Meshes: APPJ treatment settings were used as described previously,[24] with the following modifications: The APPJ was mounted in a 3D printer (FlSun i3 Prusa) modified in-house (Figure S1, Supporting Information). Marlin firmware was edited and uploaded with Arduino. The printer was operated with Repetier software, and codes were made in-house using Matlab. The resonance frequency for the system was 32.0 kHz. APPJ treatment was conducted at three different speeds, slow (2.50 m min^{-1}), medium (3.05 m min^{-1}), or fast (3.60 m min^{-1}). APPJ treatment was conducted in parallel lines spaced 5 mm apart. For all experiments, treatment was conducted on both sides of the MEW meshes, using forceps to transfer between sides. Where samples were rectangular, APPJ treatment lines were parallel to the longer side.

X-Ray Photoelectron Spectroscopy (XPS): A Thermo Scientific™ K-Alpha+™ spectrometer (Thermo Fisher Scientific, UK) was used for XPS measurements; and Thermo Avantage software (version 5.9902, Thermo Fisher Scientific, UK) was used for collecting data and analyzing the data. The X-ray source was a monochromatic Al K-Alpha (1486.6 eV) with 12.0 eV nominal operating voltage. Twenty scans were collected for survey spectra with a step size of 1.0 eV; and for carbon (C1s) high-resolution spectra with a step size of 0.1 eV. The spot size was 40 µm. Mesh samples with the size of 10 mm × 5 mm made of 50 layers with 400 µm fiber spacing were used for these measurements. For the XPS measurements, samples were mounted on 2D 8 × 12 mm indium pieces for assisting in *z*-axis precision. Samples were squashed with a metal spatula and secured with carbon tape at each of the four corners, and five measurements were taken per sample. Two samples were measured per condition. Fitting of C1s high resolution spectra was conducted using a linear background and a combination of Gaussian (70%) and Lorentzian (30%) line shapes. The presented spectra are representative for each condition. Errors displayed are standard errors of the mean obtained from at least three data points, each corresponding to a single measurement.

Dynamic Wettability Analysis: The dynamic wettability of APPJ-treated samples (10 × 5 mm mesh with 100 layers and 400 µm fiber spacing) was investigated using 5 µL water droplets from an Attension Theta tensiometer (Biolin Scientific). Dynamic wettability was considered a more effective measure of hydrophilicity for porous 3D scaffolds than measuring water contact angles.[35,36] Samples were recorded for at least 180 s after the droplets touched the surfaces. At least three drops were measured per sample, and at least two samples were measured per condition.

MEW Microfiber Morphology Analysis: PCL meshes (10 × 5 mm mesh with 50 layers and 400 µm fiber spacing) before and after APPJ treatment ($n = 1$) were first coated with a thin layer of Au/Pd using a sputter coater (SC7620 Quorum). Scanning electron microscopy (SEM) images of the coated PCL meshes were then obtained using a Phenom XL SEM with the Secondary Electron (SE) detector. The chamber pressure was kept below 1 Pa, while an acceleration voltage of 10 kV was applied at a working distance of 5 mm.

Covalent Protein Immobilization: Following APPJ functionalization of MEW microfiber meshes, the meshes were submerged in TGF (TGFβ1, Peprotech, USA) in PBS solutions with different concentrations (10, 100, 500, or 1000 ng mL^{-1}) for 24 h at 4 °C. 10 and 1000 ng mL^{-1} concentrations were used for immunofluorescent detection of immobilized TGF. All

concentrations were used for the first enzyme linked immunosorbent assay (ELISA) and in vitro optimization of TGF concentration for this study. The 1000 ng mL^{-1} condition was used for the second ELISA and the final in vitro experiments.

Immunofluorescence Detection of Immobilized Protein: Following APPJ functionalization (fast speed) and subsequent immobilization (10 and 1000 ng mL^{-1}), MEW meshes were washed before species-specific blocking was carried out using 10% normal goat serum for 30 min. Anti-TGF primary antibody incubation (1:100; Abcam) was carried out overnight at 4 °C. Secondary antibody incubation (1:350; Abcam) proceeded the following day for 2 h at 24 °C in the dark. Tween20 detergent (0.1%) was used to remove unbound antibodies from the samples prior to mounting using Fluoromount G (SouthernBiotech). Samples were imaged using a Leica Sp8 confocal microscope (n = 2). Maximum projections of constant volumes (54 µm with 3 µm voxel size) were processed for visual depiction of TGF immobilization and single images were used for the pixel value quantification. Integrated density of grey-scale look-up table was measured using ImageJ to quantify fluorescence intensity by calculating the total pixel value for each image. The total pixel value of meshes that did not contain immobilized protein was used to subtract any potential autofluorescence detected from the PCL. Error bars shown are standard deviation of two samples.

ELISA Analysis for Quantification of Covalent Protein Immobilization: Following APPJ functionalization, 5 mm diameter MEW meshes were punched and submersed for 2 h at 24 °C in different concentrations of TGF (0, 10, 100, 500, 1000, or 2000 ng mL^{-1}). Untreated meshes were submersed in 0 or 2000 ng mL^{-1} only. Meshes were rinsed briefly in PBS before washing with 5% (w/v) sodium dodecyl sulfate (SDS) for 1 h at 37 °C on an orbital shaker (80 rpm) to remove non-covalently immobilized TGF. Meshes were then rinsed six times in fresh PBS followed by blocking with 3% (w/v) BSA in PBS for 30 min at 24 °C. Anti-TGF primary antibody (rabbit 1:250; Abcam) incubation was carried out for 1 h at 24 °C. Meshes were washed four times in wash buffer (0.5% Tween 20, 0.5% BSA in PBS). Secondary antibody Goat Anti-rabbit IgG HRP (1:1000; Abcam) incubation was carried out for 1 h at room temperature. Meshes were washed six times in wash buffer. Meshes were then incubated with 50 µL 1-Step Ultra TMB substrate (ThermoFisher Scientific) in a clean 96 well plate for 20 min at room temperature in the dark. Meshes were removed from wells prior to addition of 50 µL 2M H_2SO_4 stop solution. Absorbance was read at 450 nm using a microplate reader (Tecan, infinite M1000). This protocol was developed in response to issues creating false signals, namely topography changes due to PCL swelling in solution and in response to SDS that revealed new unblocked surfaces followed by non-specific physisorption of the antibodies on the new unblocked surfaces. A single measurement was taken per sample, and three samples were measured per condition, corresponding to three different meshes. Errors shown are standard deviation using three samples. The extent of TGF immobilization was statistically compared with Bonferroni's post hoc test (concentration and speed).

ELISA Analysis for Protein Loading Efficiency and Elution: APPJ-treated and untreated 5 mm diameter MEW meshes were punched and submersed for 24 h at 4 °C in 400 µL of 1,000 ng mL^{-1} TGF solution with 0.1% BSA. Two meshes were submerged per Eppendorf tube in order to increase the signal strength. Three sets of meshes were measured per condition. Meshes from the '0 day' condition were transferred to new Eppendorf tubes after incubation and frozen at –80 °C for storage until end point ELISA. Meshes from the '28 day' condition were transferred to 0.1% BSA in PBS solution and placed in incubator at 37 °C. The buffer solution was changed after every 7 days and eluted protein was collected. All collected solutions were frozen at –80 °C for storage until end point ELISA. Hundred microliters of '0 day' immobilization solution and 7, 14, 21, and 28 day eluted protein solutions were incubated in an ELISA plate (Immulon 2 HB, ThermoFisher Scientific) overnight at 4 °C. Meshes and ELISA plate wells were rinsed two times with fresh PBS followed by blocking with 1% (w/v) BSA in PBS for 1 h at 24 °C. All samples were washed three times in wash buffer (0.05% Tween 20, 0.05% BSA in PBS). Anti-TGF primary antibody (rabbit 1:500; Abcam) incubation was carried out for 1 h at 24 °C. All samples were washed three times in wash buffer. Secondary antibody Goat Anti-rabbit IgG HRP (1:1000; Abcam) incubation was carried out for 1 h at room temperature. All samples were washed three times in wash buffer. Meshes were transferred to empty wells of the ELISA plate, then 100 µL 1-Step Ultra TMB substrate (ThermoFisher Scientific) was added to all wells and incubated for 30 min at 24 °C in the dark. Meshes were removed from wells prior to addition of 100 µL 2 M H_2SO_4 stop solution. Absorbance was read at 450 nm using a microplate reader (Tecan, infinite M1000). Errors displayed are standard errors of the mean obtained from three data points. The extent of TGF loading efficiency and elution were statistically compared with Bonferroni's post hoc test (time and treatment).

Protein Immobilization Density Calculation: Average protein density was calculated by dividing the average TGF loaded onto meshes by the surface area of those meshes. Mesh surface area was calculated by first modeling the mesh as a collection of cylinders in a rectangular prism arrangement, then applying a 'square to circle' conversion factor to adjust the surface area to the cylindrical shape of the real meshes. Two 5 mm diameter meshes with 50 layers, 400 µm fiber spacing, and 10 µm fiber thickness diameter were used per data point. The conversion factor was calculated to be 0.785 by dividing the area for a circle by that of a square. It was assumed that one set of fibers in x and y were included per layer, that 10% of the fibers are hidden by contact with other fibers as part of the mesh layering,[48] and that the fibers were smooth. Errors described are standard errors of the mean obtained from three data points.

Mesenchymal Stromal Cells (MSCs) Expansion and Seeding on MEW Microfiber Meshes: Equine MSCs were isolated from bone marrow aspirate of a healthy horse with approval from the local animal ethics committee as previously described.[49,50] MSCs were thawed and expanded in alpha-minimum essential medium (α-MEM, Life Technologies), supplemented with 10% fetal bovine serum, 100 U mL^{-1} penicillin, 100 µg mL^{-1} streptomycin, 0.2 mM L-ascorbic acid-2-phosphate (ASAP) and 1 ng mL^{-1} basic fibroblast growth factor (bFGF, R&D Systems). The treatment groups consisted of APPJ-functionalized meshes with (+APPJ +TGF) and without immobilized TGF (+APPJ –TGF), as well as untreated meshes with TGF supplemented in the medium (–APPJ +TGF) and without TGF supplementation (–APPJ –TGF). Mesh discs were biopsy punched (∅ = 5 mm), sterilized, and protein immobilized where appropriate. All samples were submerged in MSC expansion medium for 24 h at 4 °C prior to seeding. There were eight samples from each treatment group per timepoint (1, 7, 11, 14, and 28 days of culture) seeded with cells and one empty sample per timepoint to act as a blank for biochemical assays. MSCs (passage 3) were resuspended 1.6×10^7 cells mL^{-1} in basic chondrogenic culture medium (Dulbecco's modified eagle medium (DMEM, Life Technologies), supplemented with 100 U mL^{-1} penicillin, 100 µg mL^{-1} streptomycin, 0.2 mM ASAP, 1:100 ITS premix (Corning), and 40 ng mL^{-1} Dexamethasone (Sigma)). The concentrated cell suspension was seeded into dried meshes in 30 µL droplets (4.8×10^5 cells/mesh) and left for 5 h to allow for cellular attachment to PCL microfibers. Following microscopic visual attachment of cells, 1 mL of respective culture medium (i.e., basic chondrogenic culture medium containing or excluding TGF was added to each sample in 24-well plates. +APPJ +TGF, +APPJ –TGF, and –APPJ –TGF groups were cultured in basic chondrogenic culture medium (mentioned above). The –APPJ +TGF group was cultured in basic chondrogenic culture medium, supplemented with 10 ng mL^{-1} TGF (TGFβ1, Peprotech, USA), which was freshly thawed and supplied at each media change. Samples were cultured for a 28 day period, with media refreshed two times per week.

Mechanical Testing: The mechanical properties of both cell free and cell laden fibrous meshes were assessed by uniaxial tensile and unconfined compression testing, respectively. Both tests were performed on a MultiTest-2.5-dv system (Mecmesin, UK) equipped with a 250N load cell. Tests were conducted at a constant rate of 1 mm min^{-1} at room temperature. For tensile tests, rectangular strips (11 × 7 mm) of APPJ-treated 3D microfiber meshes (400 µm fiber spacing) at three different speeds (slow, medium, and fast) were used; while for compression tests, cylindrical cultured meshes (6 mm diameter, 0.8 ± 0.2 mm thickness)

following 28 days of culture were used. Tensile and compressive modulus were determined from engineering stress–strain curves using a least square fitting of the slope of the stress–strain curves between 0–20% strain for tensile tests and 10–15% strain for compressive tests. At least three samples (different constructs) for each type of mechanical test and group were tested.

Histology and Immunohistochemistry: After 1, 7, 11, 14, and 28 days of culture, samples ($n = 2$) were fixed in formalin for 30 min and then transferred to 0.1% eosin (in 4% formalin) for general tissue staining. Samples were subsequently embedded in 4% agarose to minimize loss of samples prior to standard tissue processing and embedding in paraffin. Following paraffin embedding, samples were cut at 5 µm thickness and stained with safranin-O for glycosaminoglycan visualization,[51] fast green for cytoplasm and collagen and Weigert's hematoxylin for cell nuclei. Immunohistochemical staining of collagen type II was also performed on the paraffin sections as previously described[49] using the primary antibody II-II6B3 (DSHB, USA). Histology images were made of mounted sections in 3x random locations using a bright field microscope.

Biochemical Assays: Metabolic assays were performed after 1, 7, 11, 14, and 28 days of culture on the same samples ($n = 6$) using a resazurin assay (resazurin sodium salt, Alfa Aesar, Germany). A working solution was prepared in chondrogenic differentiation medium (–TGF) containing 44.11 µM resazurin sodium salt. Briefly, samples were incubated, protected from light, for 4 h at 37 °C. Fluorescence was measured in duplo with excitation at 544 nm and emission at 620 nm. To quantify glycosaminoglycan (GAG) production during the culture period, samples were taken after 1, 7, 11, 14, and 28 days of culture and subsequently freeze dried ($n = 6$). Samples were then digested using 50 µL of papain buffer consisting of 0.2 M NaH_2PO_4 and 0.01 M EDTA*$2H_2O$ with a pH of 6.0, mixed with 7.75 units mL^{-1} papain solution and 1.57 mg mL^{-1} cysteine HCl. Samples were digested overnight at 60 °C and then assayed for DNA and GAG content using the Picogreen assay kit (Thermo Fisher Scientific) and dimethyl methylene blue assay (DMMB, Sigma), respectively. Briefly, DMMB solution was prepared in-house with a pH of 3. Chondroitin sulphate C was used to prepare a standard curve with concentrations from 0 to 10 µg mL^{-1}. Excitation was measured in duplo at 525 and 595 nm wavelengths, dividing the 525 nm measurement by the 595 nm measurement before subtracting the blank and performing subsequent analysis. GAG production was normalized against DNA content for each sample to normalize for cell number variation.

Quantitative Real-Time Polymerase Chain Reaction (qRT-PCR): After 1, 7, 11, 14, and 28 days, cultured meshes were collected ($n = 6$) and lysed using 0.5 mL per sample TRIzol reagent (Thermo Fisher Scientific). mRNA was isolated using 20% chloroform and extracted from the aqueous phase. Subsequent quantification was performed using a NanoDrop ND100 spectrophotometer (Thermo Fisher Scientific) at 260/280 nm. The iScript cDNA Synthesis Kit was used to synthesize cDNA using the manufacturer's instructions. PCR analysis of collagen type I (COL1A1), collage type II (COL2A1), collagen type X (COLXA1), transcription factor primer D (SOX9), and aggrecan (ACAN) were completed with a Bio-Rad CFX96 Real-Time PCR Detection System (Bio-Rad) using FastGreen SYBR Green Master mix (Sigma–Aldrich). Hypoxanthine Phosphoribosyl transferase 1 (HPRT) was used as the housekeeping gene reference for the expression of the target genes. CT-values higher than the 40th cycle were considered undetectable and thus not plotted. The relative fold change was determined using the $2^{-\Delta\Delta CT}$ method using the mean ΔCT value of the D7, +APPJ –TGF group as the standard. Chondrogenic index was calculated by dividing COL2A1 fold change mean by COL1A1 fold change mean. The primers that were used are listed in Table S1 (Supporting Information) and were designed and validated elsewhere.[26]

Statistical Analysis: Statistical analysis was performed using GraphPad Prism 9.2.0. Significance was determined using p-value < 0.05 unless otherwise stated. The difference in atomic concentration of peak-fitted C 1s components was analyzed using a paired t test. ELISA immobilization and loading efficiency measurements were analyzed for variance using a two-way analysis of variance (ANOVA) with Bonferroni's post hoc test, with concentration and speed or time and treatment, respectively. The difference in calculated moduli was statistically analyzed using one-way ANOVA and subsequent post hoc Tukey multiple-comparisons analysis. The normalized production of GAGs was statistically analyzed using two-way ANOVA and subsequent post hoc Tukey multiple-comparisons analysis. Error bars shown are standard deviation of six samples. The fold change of target genes was statistically analyzed using two-way ANOVA and subsequent post hoc Tukey multiple-comparisons analysis.

Supporting Information

Supporting Information is available from the Wiley Online Library or from the author.

Acknowledgements

M.J.A. and O.L. contributed equally to this work. B.A. and M.C. are shared senior authors. The authors would like to kindly acknowledge the financial support from the Gravitation Program "Materials Driven Regeneration", funded by the Netherlands Organization for Scientific Research (024.003.013), the EU's H2020 Marie Skłodowska-Curie RESCUE co-fund grant (#801540), the Jennifer Foong Scholarship for Biomedical Research, and an Office of Global Engagement Partnership Collaboration Award between the University of Sydney, Utrecht University, and the Australian Research Council (FL190100216; DP190103507; and DE210100662). This work was also supported by the partners of Regenerative Medicine Crossing Borders and powered by Health ~Holland, Top Sector Life Sciences & Health. The authors would like to thank I. Dokter for assistance with running qPCRs and M. van Rijen for histology expertise. The DSHB Hybridoma Product II-II6B3 developed by T.F. Linsenmayer was obtained from the Developmental Studies Hybridoma Bank, created by the NICHD of the NIH and maintained at The University of Iowa, Department of Biology, Iowa City, IA 52242.

Conflict of Interest

The authors declare no conflict of interest.

Data Availability Statement

The data that support the findings of this study are available from the corresponding author upon reasonable request.

Keywords

atmospheric-pressure plasma, cartilage, melt electrowriting, protein immobilization, stem cell differentiation, technology convergence, transforming growth factor beta

Received: June 9, 2022
Revised: October 15, 2022
Published online: November 22, 2022

[1] Y. Krishnan, A. J. Grodzinsky, *Matrix Biol.* **2018**, *71*, 51.
[2] J. Becerra, J. A. Andrades, E. Guerado, P. Zamora-Navas, J. M. López-Puertas, A. H. Reddi, *Tissue Eng. – Part B Rev.* **2010**, *16*, 617.

[3] L. Peterson, M. Brittberg, I. Kiviranta, E. L. Åkerlund, A. Lindahl, *Am. J. Sports Med.* **2002**, *30*, 2.
[4] S. Marlovits, P. Zeller, P. Singer, C. Resinger, V. Vécsei, *Eur. J. Radiol.* **2006**, *57*, 24.
[5] H. B. Schuette, M. J. Kraeutler, E. C. McCarty, *Orthop. J. Sport. Med.* **2017**, *5*, 1.
[6] S. C. Mastbergen, D. B. F. Saris, F. P. J. G. Lafeber, *Nat. Rev. Rheumatol.* **2013**, *9*, 277.
[7] M. Castilho, V. Mouser, M. Chen, J. Malda, K. Ito, *Acta Biomater.* **2019**, *95*, 297.
[8] V. H. M. Mouser, R. Levato, L. J. Bonassar, D. D. D'Lima, D. A. Grande, T. J. Klein, D. B. F. Saris, M. Zenobi-Wong, D. Gawlitta, J. Malda, *Cartilage* **2017**, *8*, 327.
[9] J. Visser, F. P. W. Melchels, J. E. Jeon, E. M. Van Bussel, L. S. Kimpton, H. M. Byrne, W. J. A. Dhert, P. D. Dalton, D. W. Hutmacher, J. Malda, *Nat. Commun.* **2015**, *6*, 6933.
[10] G. Zhen, X. Cao, *Trends Pharmacol. Sci.* **2014**, *35*, 227.
[11] W. Wang, D. Rigueur, K. M. Lyons, *Birth Defects Res. Part C Embryo Today Rev.* **2014**, *102*, 37.
[12] L. A. Fortier, J. U. Barker, E. J. Strauss, T. M. McCarrel, B. J. Cole, *Clin. Orthop. Relat. Res.* **2011**, *469*, 2706.
[13] L. S. Dolci, A. Liguori, A. Merlettini, L. Calzà, M. Castellucci, M. Gherardi, V. Colombo, M. L. Focarete, *J. Phys. D. Appl. Phys.* **2016**, *49*, 274003.
[14] L. S. Wong, F. Khan, J. Micklefield, *Chem. Rev.* **2009**, *109*, 4025.
[15] C. Stewart, B. Akhavan, S. G. Wise, M. M. M. Bilek, *Prog. Mater. Sci.* **2019**, *106*, 100588.
[16] S. L. Hirsh, D. R. McKenzie, N. J. Nosworthy, J. A. Denman, O. U. Sezerman, M. M. M. Bilek, *Colloids Surf., B* **2013**, *103*, 395.
[17] L. Vroman, A. L. Adams, *J. Biomed. Mater. Res.* **1969**, *3*, 43.
[18] E.-H. Lim, J. P. Sardinha, S. Myers, M. Stevens, *Arch. Plast. Surg.* **2013**, *40*, 676.
[19] F. F. Chen, M. D. Smith, *In Van Nostrand's Scientific Encyclopedia* **1984**.
[20] M. M. M. Bilek, M. Vandrovcová, A. Shelemin, A. Kuzminova, O. Kylián, H. Biederman, L. Bačáková, A. S. Weiss, *Appl. Surf. Sci.* **2020**, *518*, 146128.
[21] F. Fanelli, F. Fracassi, *Surf. Coat. Technol.* **2017**, *322*, 174.
[22] C. Tendero, C. Tixier, P. Tristant, J. Desmaison, P. Leprince, *Spectrochim. Acta Part B At. Spectrosc.* **2006**, *61*, 2.
[23] X. Lu, G. V. Naidis, M. Laroussi, S. Reuter, D. B. Graves, K. Ostrikov, *Phys. Rep.* **2016**, *630*, 1.
[24] S. K. Alavi, O. Lotz, B. Akhavan, G. Yeo, R. Walia, D. R. McKenzie, M. M. Bilek, *ACS Appl. Mat. Interfaces* **2020**, *14*, 38730.
[25] H. Najafi-Ashtiani, B. Akhavan, F. Jing, M. M. Bilek, *ACS Appl. Mater. Interfaces* **2019**, *11*, 14871.
[26] L. Utomo, Y. M. Bastiaansen-Jenniskens, J. A. N. Verhaar, G. J. V. M. van Osch, *Osteoarthr. Cartil.* **2016**, *24*, 2162.
[27] I. Trizio, F. Intranuovo, R. Gristina, G. Dilecce, P. Favia, *Plasma Process. Polym.* **2015**, *12*, 1451.
[28] S. Surucu, K. Masur, H. Turkoglu Sasmazel, T. Von Woedtke, K. D. Weltmann, *Appl. Surf. Sci.* **2016**, *385*, 400.
[29] M. Cámara-Torres, R. Sinha, P. Scopece, T. Neubert, K. Lachmann, A. Patelli, C. Mota, L. Moroni, *ACS Appl. Mater. Interfaces* **2021**, *13*, 3631.
[30] U. Little, F. Buchanan, E. Harkin-Jones, B. Graham, B. Fox, A. Boyd, B. Meenan, G. Dickson, *Acta Biomater.* **2009**, *5*, 2025.
[31] Z. Ma, W. He, T. Yong, S. Ramakrishna, *Tissue Eng.* **2005**, *11*, 1149.
[32] C. T. Tran, T. J. Raeber, B. J. Murdoch, A. J. Barlow, J. G. Partridge, D. G. McCulloch, D. R. McKenzie, *J. Appl. Phys.* **2019**, *125*, 075302.
[33] K. Fricke, K. Duske, A. Quade, B. Nebe, K. Schroder, K. Weltmann, T. von Woedtke, *IEEE Trans. Plasma Sci.* **2012**, *40*, 2970.
[34] K.-Y. Law, H. Zhao, in *Surface Wetting*, Springer International Publishing, Cham **2016**.
[35] M. J. Hawker, A. Pegalajar-Jurado, E. R. Fisher, *Plasma Process. Polym.* **2015**, *12*, 846.
[36] E. R. Fisher, *ACS Appl. Mater. Interfaces* **2013**, *5*, 9312.
[37] D. P. Dowling, M. Donegan, P. J. Cullen, V. J. Law, V. Milosavljevic, *IEEE Trans. Plasma Sci.* **2014**, *42*, 2426.
[38] A. Maffei, N. Michieli, P. Brun, A. Zamuner, A. Zaggia, M. Roso, B. Kalinic, E. Verga Falzacappa, P. Scopece, S. Gross, M. Dettin, A. Patelli, *Appl. Surf. Sci.* **2020**, *507*, 144713.
[39] D. Mance, R. Wiese, T. Kewitz, H. Kersten, *Eur. Phys. J. D* **2018**, *72*, 98.
[40] T. D. Brown, P. D. Dalton, D. W. Hutmacher, *Prog. Polym. Sci.* **2016**, *56*, 116.
[41] A. Charuchinda, R. Molloy, J. Siripitayananon, N. Molloy, M. Sriyai, *Polym. Int.* **2003**, *52*, 1175.
[42] I. Castilla-Cortázar, J. Más-Estellés, J. M. Meseguer-Dueñas, J. L. Escobar Ivirico, B. Marí, A. Vidaurre, *Polym. Degrad. Stab.* **2012**, *97*, 1241.
[43] X. Wei, C. Gong, M. Gou, S. Fu, Q. Guo, S. Shi, F. Luo, G. Guo, L. Qiu, Z. Qian, *Int. J. Pharm.* **2009**, *381*, 1.
[44] M. Sarem, O. Otto, S. Tanaka, V. P. Shastri, *Stem Cell Res. Ther.* **2019**, *10*, 10.
[45] Z. X. Xu, T. Li, Z. M. Zhong, D. S. Zha, S. H. Wu, F. Q. Liu, W. De Xiao, X. R. Jiang, X. X. Zhang, J. T. Chen, *Biopolymers* **2011**, *95*, 682.
[46] R. Ghobeira, C. Philips, L. Liefooghe, M. Verdonck, M. Asadian, P. Cools, H. Declercq, W. H. De Vos, N. De Geyter, R. Morent, *Appl. Surf. Sci.* **2019**, *485*, 204.
[47] P. Behrendt, Y. Ladner, M. J. Stoddart, S. Lippross, M. Alini, D. Eglin, A. R. Armiento, *Am. J. Sports Med.* **2020**, *48*, 210.
[48] M. Castilho, G. Hochleitner, W. Wilson, B. van Rietbergen, P. D. Dalton, J. Groll, J. Malda, K. Ito, *Sci. Rep.* **2018**, *8*, 1245.
[49] R. Levato, W. R. Webb, I. A. Otto, A. Mensinga, Y. Zhang, M. van Rijen, R. van Weeren, I. M. Khan, J. Malda, *Acta Biomater.* **2017**, *61*, 41.
[50] J. Visser, D. Gawlitta, K. E. M. Benders, S. M. H. Toma, B. Pouran, P. R. van Weeren, W. J. A. Dhert, J. Malda, *Biomaterials* **2015**, *37*, 174.
[51] L. Rosenberg, *J. Bone Jt. Surg.* **1971**, *53*, 69.